

# Structural transition, spontaneous formation of strong singlet dimers and metamagnetism in $S = 3/2$ magnetoelastic spin chains

C. J. Gazza,<sup>1</sup> A. A. Aligia,<sup>2</sup> A. O. Dobry,<sup>1</sup> G. L. Rossini,<sup>3</sup> and D. C. Cabra<sup>3</sup>

<sup>1</sup>*IFIR-CONICET and Facultad de Ciencias Exactas,  
Ingeniería y Agrimensura, Universidad Nacional de Rosario, Argentina*

<sup>2</sup>*Instituto de Nanociencia y Nanotecnología, CNEA-CONICET,  
GAIDI, Centro Atómico Bariloche, 8400 Bariloche, Argentina*

<sup>3</sup>*IFLySiB-CONICET and Departamento de Física, Universidad Nacional de La Plata, Argentina*  
( $\Omega$ Dated: September 23, 2024)

We study a one-dimensional antiferromagnetic-elastic model with magnetic ions having spin  $S = 3/2$ . By extensive DMRG computations and complementary analytical methods, we uncover a first-order transition from a homogeneous or weakly-dimerized phase (a situation that could be similar to the well known  $S = 1/2$  spin-Peierls effect) to a highly distorted phase, driven by the spin-phonon coupling  $\lambda$ . The striking characteristic of the second phase, present at large  $\lambda$ , is the appearance of weakly ferromagnetic (FM) couplings alternating with strong antiferromagnetic (AFM) ones (we dub it FM-AFM phase) with a ground state close to a direct-product state of singlet dimers sitting on the AFM bonds. The behavior of the spin gap in both phases is studied by DMRG computation and contrasted with bosonization predictions and perturbation theory around the direct product of dimers. In the FM-AFM phase robust magnetization plateaus and metamagnetic jumps show under magnetic fields.

The novel phase could be realized in 5d oxides of current interest, with giant spin-phonon coupling. Potential applications of the transition would be associated to the possibility of tuning the transition by external parameters such as striction, magnetic or electric fields, or alloying.

PACS numbers: 75.85.+t, 75.10 Jm, 75.10 Pq

## I. INTRODUCTION

It is by now well established that a one dimensional spin  $S = 1/2$  system coupled to the lattice has an instability towards dimerization in a wide range of the model parameters, the so-called spin-Peierls (SP) instability. Theoretical understanding [1] and numerical confirmation [2] have been presented years ago. The phenomenon is robust against various details in the magnetic exchange [3] and in the elastic coupling to the lattice [4,5].

This instability has strong consequences [6] in materials such as the (TMTTF)<sub>2</sub>X Fabre salts and related salts with the o-DMTTF donors as well as in the inorganic material CuGeO<sub>3</sub> [7], where most of the theoretical predictions have been experimentally tested in different scenarios.

Such kind of magneto-elastic instabilities have also been studied in more general situations, *e.g.* in the presence of an external magnetic field [8,9], in quasi one-dimensional arrays such as spin ladders, in chains of magnetic ions with spin higher than  $1/2$  [10], etc. The spin-Peierls transition has been also thoroughly studied in two-dimensional systems, either bipartite as the square lattice or in frustrated ones [11].

Regarding the study of magneto-elastic spin chains with  $S > 1/2$ , there has been intense research in connection with the well-known Haldane conjecture [12] which states strong differences between integer or half-odd-integer  $S$ . Based on a low-energy field theory mapping [13,14] it was conjectured that the SP instability could also take place in chains with half odd-integer spin

greater than  $S = 1/2$ . This has been further supported numerically [15] and theoretically using the non-Abelian bosonization mapping [16]. But in spite of the theoretical efforts, numerical evidence is hardly conclusive for chains with spin higher than  $1/2$ , partly due to the additional complexity associated to the increasing dimension of the local Hilbert space. In an early work [10], it was argued that for integer spin the SP instability would be generically absent, while it would survive for half odd-integer spin chains. These early results have been obtained in very short chains and the extrapolations are at most qualitative. As a consequence, the complete phase diagram has not been established so far, and the existence of a magneto-elastic instability for  $S > 1/2$  is still controversial.

More recently a SP-like structural transition has been claimed to be relevant in the description of many multiferroic systems such as some double perovskites, manganites, nickelates, etc. where a simultaneous sudden increase of the magnetization along with an equally abrupt decrease of the electric polarization is experimentally observed [17–21]. This phenomenon has been theoretically studied in low-dimensional models [22,23] where it was shown that the interplay between magnetic and electric dipoles mediated by the elastic degrees of freedom explains most of the experimentally observed features.

Motivated by the ubiquitous relevance of the SP transition in magneto-elastic systems, and the apparent validity of the Haldane conjecture, in the present paper we focus on the  $S = 3/2$  case.

Analyzing the model in absence of magnetic field for

a wide range of the spin-phonon coupling  $\lambda$ , aside from the elusive question of the existence of a SP instability for weak  $\lambda$ , we find a feature not present in the  $S = 1/2$  physics which is the main message in this work: a first-order structural transition as a function of the spin-phonon coupling from a homogeneous/weakly-dimerized phase with antiferromagnetic exchanges at low coupling (which would be consistent with the field theoretical expectations [13,14,16]) into a strongly dimerized phase with alternating ferro- and antiferro-magnetic exchange interactions (dubbed here as FM-AFM phase) realized at strong coupling. The two distinct regimes could be observed in different materials, according to their intrinsic spin-phonon coupling, but more interestingly the transition could be driven by a variety of parameters such as striction, magnetic or electric fields, etc.

The uncovered FM-AFM phase is potentially relevant for multiferroic applications whenever a tailoring of  $\lambda$  leads to a giant variation of the magnetic susceptibility. The presence of the first-order transition, and the associated large change in the crystal structure, could produce a noticeably drastic jump in both magnetization and electric polarization in improper type II multiferroic materials whenever half-odd-integer higher spins were involved.

The paper is organized as follows: in Section II we introduce the model, describe the numerical approach, and present clear evidence of the first-order transition from extensive DMRG computations. We also discuss the response of the model to external magnetic fields. In Section III we discuss analytical support from perturbation theory applied to the decoupled dimers regime, which provides a valuable description of the strongly dimerized phase. In Section IV we review the question of the low spin-phonon coupling regime and the existence of a spin-Peierls instability in the  $S = 3/2$  chain at the light of our numerical results. Section V provides a summary, discusses the findings, and outlines potential applications.

## II. THE MODEL AND NUMERICAL RESULTS

### A. Model Hamiltonian

We consider a magneto-elastic spin chain with local spins  $S = 3/2$ . The magnetic sector is described by nearest-neighbor antiferromagnetic exchange with Hamiltonian given by

$$H_{\text{spin}} = \sum_i J_i \mathbf{S}_i \cdot \mathbf{S}_{i+1} - h^z \sum_i S_i^z \quad (1)$$

where  $\mathbf{S}_i$  is the magnetic moment of an ion at site  $i$  ( $1 \leq i \leq N$  in a chain of  $N$  sites and periodic boundary conditions) and  $h^z$  is a homogeneous external magnetic field. A minimal coupling to the lattice is given by distortion modulated exchange couplings

$$J_i = J [1 - \alpha(u_{i+1} - u_i)] \quad (2)$$

where  $u_i$  describes the displacement of ion  $i$  from its regular lattice position. That is,  $J_i$  depends linearly on the bond distortion  $\delta_i \equiv u_{i+1} - u_i$  through a (dimensionfull) spin-phonon coupling  $\alpha$ .

The lattice degrees of freedom will be described by their energy cost in the adiabatic limit, under the assumption that phonon frequencies are much smaller than  $J$ . We choose here the so-called Einstein-site phonon (ESP) model [5] which considers a quadratic energy arising from displacement of magnetic ions from their equilibrium positions (in absence of magnetic interactions),

$$H_{\text{latt}} = \frac{K}{2} \sum_i u_i^2 \quad (3)$$

describing a dispersionless optical phonon branch.

It is convenient at this point to introduce dimensionless parameters which will be used in what follows. We define  $\tilde{u}_i = \alpha u_i$  and  $\tilde{h}^z = h^z/J$ , setting the energy scale  $J = 1$ . The model Hamiltonian  $H = H_{\text{spin}} + H_{\text{latt}}$  then reads

$$H/J = \sum_i \left[ (1 - (\tilde{u}_{i+1} - \tilde{u}_i)) \mathbf{S}_i \cdot \mathbf{S}_{i+1} + \frac{1}{2\lambda} \tilde{u}_i^2 - \tilde{h}^z S_i^z \right] \quad (4)$$

where  $\lambda = J\alpha^2/K$  is the already mentioned dimensionless spin-phonon coupling. Notice that the length scale is given by  $1/\alpha$ , not by the lattice spacing  $a$  frequently used elsewhere.

### B. Self consistent DMRG approach

We follow a numerical approach to the full Hamiltonian in Eq. (4) based on a self-consistent adiabatic procedure to minimize the total energy [2]. Given an initial (classical) ion displacement configuration  $u_i$  we apply DMRG methods to compute the (quantum) ground-state spin configuration. We then generate a new distortion configuration from the self-consistent equation

$$\tilde{u}_i = \lambda (\langle \mathbf{S}_{i-1} \cdot \mathbf{S}_i \rangle - \langle \mathbf{S}_i \cdot \mathbf{S}_{i+1} \rangle) \quad (5)$$

and iterate until we get a fixed point.

DMRG calculations have been implemented using the ITensor software library [24], setting the necessary maximum bond dimension to keep a truncation error cutoff of  $10^{-10}$ . In all cases we have used periodic boundary conditions.

### C. Numerical results

#### 1. First-order transition in the absence of magnetic field

Starting with  $h^z = 0$ , for the full range of the spin-phonon coupling  $\lambda$  we have found that the ground state is a spin singlet ( $S_{\text{tot}}^z = 0$ ) and exhibits a period 2 pattern of ion displacements, say  $\tilde{u}_i = (-1)^i \tilde{u}_0$ , producing

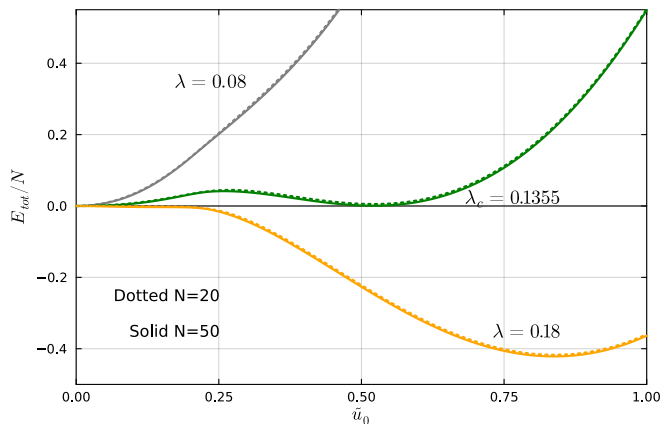


Figure 1: Total energy computed for alternating displacements as a function of their amplitude  $\tilde{u}_0$  for different values of the spin-phonon coupling  $\lambda$  (data for  $N = 20$  and  $N = 50$  sites are shown).

an alternation of short and long bond distances. But depending on  $\lambda$  we have found two strikingly different solutions, as can be seen in Fig. 1, where we show the total (magnetic plus elastic) energy for dimerized distortions as a function of the distortion amplitude  $\tilde{u}_0$  for different values of  $\lambda$ .

In the weak coupling regime (lowest  $\lambda$  in the figure) it is numerically difficult to distinguish whether the minimum energy is obtained for a homogeneous configuration or for a slight dimerization with  $\tilde{u}_0 \ll 1$  (see in Fig. 2, top panel, the presumably absence of distortions for  $\lambda = 0.08$  and discussion in Section IV). In contrast, for strong coupling (largest  $\lambda$  in Fig. 1) a highly distorted phase shows up with  $\tilde{u}_0$  of the order of 0.5 (see details in Fig. 2, top panel, for  $\lambda = 0.18$ ). In the latter case physically meaningful distortions  $u_i = \tilde{u}_i/\alpha$ , which should be much smaller than the lattice spacing  $a$ , require materials with  $\alpha \gg 1/a$ .

We describe below that there is a critical value of  $\lambda$  where a first-order transition takes place. The transition to the strongly dimerized behavior corresponds to a second local energy minimum becoming more favorable than the expected homogeneous or weakly-dimerized configuration, as illustrated in Fig. 1 by results at, below and above the critical value, estimated as  $\lambda_c \approx 0.1355$ . In the figure, we plot nearly coinciding energies for  $N = 20$  and 50 sites. The results were checked to remain stable in chains of  $N = 10, 30$  and 40 sites as well. One can see the presence of two local minima, one for vanishing or tiny  $\tilde{u}_0$  and another for large  $\tilde{u}_0$ . The minimum for large displacements becomes energetically favorable at strong coupling  $\lambda$ . We have thus found a quantum first-order transition as a function of the spin-phonon parameter  $\lambda$ , a phenomenon not present in the spin  $S = 1/2$  magneto-elastic chain.

In Fig. 3, top panel, we plot the amplitude of alternating displacements versus  $\lambda$  in the ground state of the

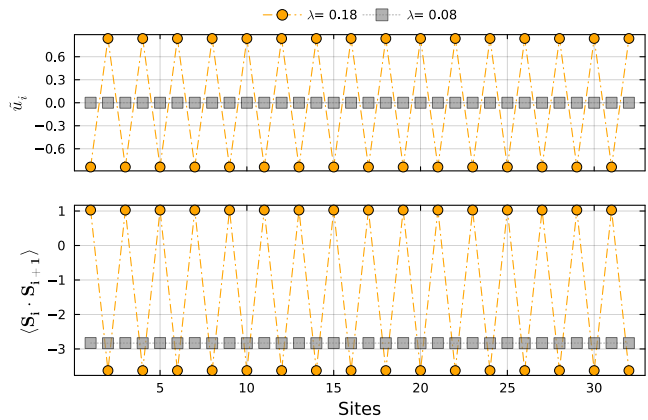


Figure 2: Elastic displacements (top panel) and spin correlations (bottom panel) for two representative values of the spin-phonon coupling  $\lambda$ . Gray squares:  $\lambda = 0.08 < \lambda_c$ . Orange circles:  $\lambda = 0.18 > \lambda_c$ .

system, for a sample chain length. One can clearly see a jump, occurring at  $\lambda_c \approx 0.1355$ . Within our numerical precision the value of  $\lambda_c$  is not sensitive to the chain length, a robust feature that should be valid in the thermodynamic limit. Beyond the critical point the displacement amplitudes jump to values larger than 0.5, making the exchange  $J_i = J[1 - (\tilde{u}_{i+1} - \tilde{u}_i)] = J(1 - 2\tilde{u}_0)$  small and negative at bonds where ions become separated. This generates an important alternation of the spin exchange between strong antiferromagnetic dimers (at short bonds) and weaker ferromagnetic interactions (at long bonds), producing a deep effect in the correlations in the strong coupling phase. In the bottom panel of Fig. 2 we show the nearest neighbors spin-spin correlations. They alternate between short and long bonds: at each short bond the correlation indeed takes a value close to  $-\frac{3}{2}(\frac{3}{2} + 1) = -\frac{15}{4}$ , which is the value corresponding to perfect singlet dimer states. For the long bonds the spin-spin correlations are in general positive (ferromagnetic). Importantly, at the transition we find  $\tilde{u}_0 = 0.5$ , so that perfect singlet dimers form in the AFM bonds with correlations  $-\frac{15}{4}$ , exactly decoupled from each other.

Were we analyzing a different magneto-elastic model, usual elsewhere [2–4,25,26], where the elastic energy is associated to bond distortions with an ad-hoc fixed length constraint (the so called bond-phonon model), we would find a spurious phase separation [27]. Such non-realistic behavior has not been observed for spin  $S = 1/2$  systems. The ESP studied here is more realistic in automatically taking into account the unavoidable correlations between bond lengths arising from the underlying three-dimensional lattice environment (see for instance [28]).

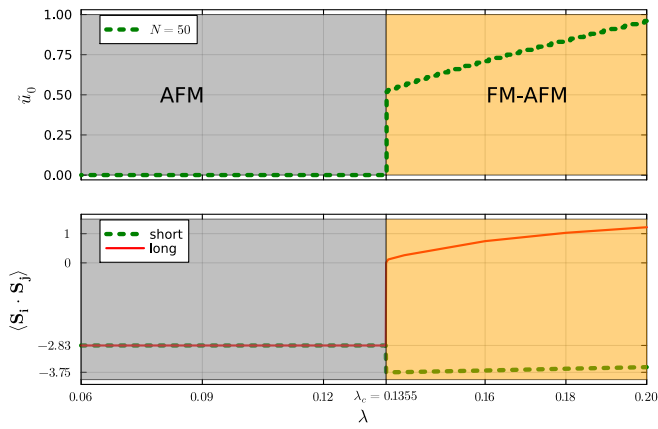


Figure 3: Amplitude of alternating displacements (top) and spin-spin correlations (bottom) in the ground-state as a function of the spin-phonon coupling.

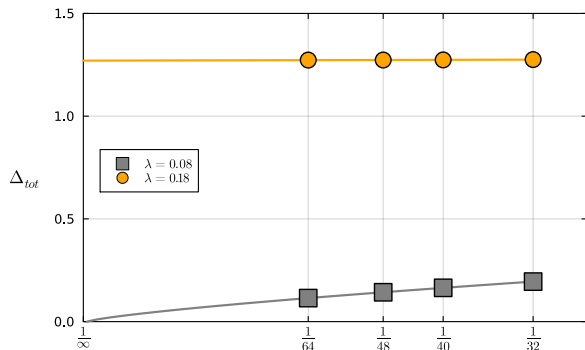


Figure 4: Finite size scaling of the spin gap for two values of  $\lambda$  at opposite sides of the transition  $\lambda = 0.08$  (circles) and  $\lambda = 0.18$  (squares).

## 2. Magneto-elastic response to external magnetic fields

*a. Spin gap:* As is well known the dimerization of exchange couplings produces a finite spin gap, defined in the present model as the difference of the total (magnetic plus elastic) energy between the lowest lying states with  $S_{\text{total}}^z = 1$  and  $S_{\text{total}}^z = 0$ , denoted here as  $\Delta_{\text{tot}}$ .

Given the abrupt onset of alternating distortions described in the previous Section, the spin gap is expected to jump from being zero or very small (see Section IV) to a finite value in the FM-AFM phase (see Section III). We show in Fig. 4 a finite size scaling of the spin gap  $\Delta_{\text{tot}}$  for the representative values of the spin-phonon coupling in each phase selected in previous figures,  $\lambda = 0.08 < \lambda_c$  and  $\lambda = 0.18 > \lambda_c$ . Solid curves correspond to  $1/N^\nu$  fitting. Below  $\lambda_c$  the extrapolated gap is zero within numerical resolution, while it is finite and almost size independent in the FM-AFM phase.

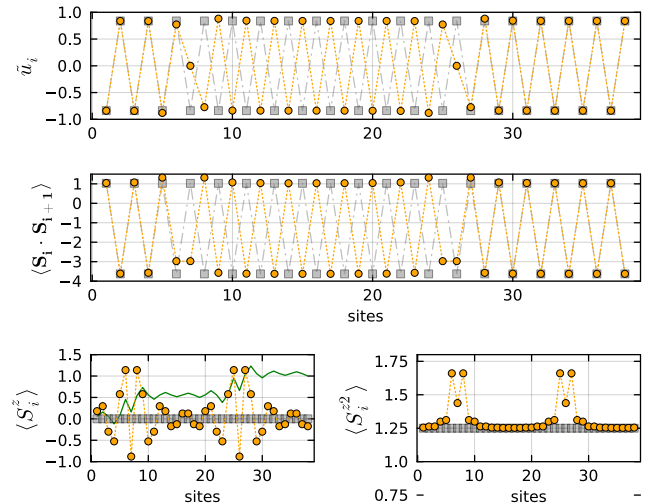


Figure 5: Comparison of observables between the lowest energy states with  $S_{\text{total}}^z = 3$  (orange circles) and  $S_{\text{tot}}^z = 0$  (gray squares), for  $\lambda = 0.18 > \lambda_c$ . Top panel: elastic ion displacements. Middle panel: nearest neighbors spin-spin correlations. Left bottom: local expectation value of the spin projection; the green line describes the accumulated magnetization (normalized to one). Right bottom: local spin anisotropy.

*b. Magnons, solitons and magnetization plateaus in the highly distorted phase:* In the highly distorted phase ( $\lambda > \lambda_c$ ) the state with  $S_{\text{total}}^z = 1$  exhibits dimerized distortions and spin correlations, very similar to the ground state  $S_{\text{total}}^z = 0$ , with a homogeneous distribution of the magnetization along the chain. The same happens in the sector  $S_{\text{total}}^z = 2$ . That is, the magnetic excitations behave as delocalized magnons.

In contrast, we have found that reaching  $S_{\text{total}}^z = 3$  (that would correspond to a rigid flip of a  $S = 3/2$  classical vector), domain walls (solitons) appear separating regions with elastic patterns that differ in that the displacements are shifted by one site. This is shown in Fig. 5, where we compare observables in the  $S_{\text{total}}^z = 3$  (orange circles) and  $S_{\text{total}}^z = 0$  (gray squares) ground states. In the top panel we show how ion displacements reconfigure with respect to the  $S_{\text{total}}^z = 0$  profile taking in different regions the two possible (one-site shifted) alternating patterns. These dimerized domains are separated by two sharp domain walls. This behavior resembles the splitting of  $S_{\text{total}}^z = 1$  magnon into a pair of  $S^z = 1/2$  localized excitations (spinons) taking place in the spin  $S = 1/2$  magneto-elastic chain [26]. There is however a difference in the detailed shape of these soliton discussed below.

In the middle panel we show the corresponding spin-spin correlations, which follow the alternation of short (antiferromagnetic) and long (ferromagnetic) bonds and the width of the domain walls.

In the left bottom panel we report the expectation value of the local  $S_i^z$  spin component. One can see that the contributions to  $S_{\text{total}}^z = 3$  are localized around the

domain walls, with a characteristic soliton shape [9]. The green line, indicating the accumulated  $\langle S^z \rangle$  contribution (normalized to one), shows that each soliton carries  $S^z = 3/2$ . Moreover, in the right bottom panel the local expectation value of  $\langle (S^z)^2 \rangle$  (1.25 for each component in the  $S_{\text{total}}^z = 0$  isotropic case) shows a spontaneous single-ion anisotropy, towards the  $z$  component in each soliton. These solitonic features in the  $S = 3/2$  spin (so similar to the  $S = 1/2$  case) suggest the existence of a  $S^z = 3/2$  spinon and deserve further investigation to be published elsewhere [29].

From the displacements in Fig. 5, top panel, one can see that the bonds around the center of domain walls are *short*, leading to three closer sites separating two nearly perfectly dimerized regions. We call this case B. On the other hand the simplest defect that could separate two dimerized regions, say case A, would be an isolated spin  $3/2$  separated by *long* bonds to the neighboring dimerized regions. While the elastic cost looks the same, case A gains magnetic energy in one more dimerized bond (AFM singlet) with respect to case B, but case B can gain energy by arranging the spins of the three sites. To estimate the energy balance assume that the displacements are  $\tilde{u} = \pm 0.5$  (near the transition) so that  $J_i = 0$  ( $2J$ ) for the long (short) bonds in the dimerized phases. To first order the singlets do not interact with the domain wall structure in the middle. In case B one has a chain of three sites interacting with  $J_B = 3/2 J$ . The energy is minimized coupling ferromagnetically the two spins at the borders leading to a total spin  $S_b = 3$  and coupling the resulting spin antiferromagnetically with the central one  $S_c = 3/2$ , leading to a total spin  $S_t = 3/2$ . A simple calculation leads to  $\mathbf{S}_b \cdot \mathbf{S}_c = -S_b(S_b+1)/2 = -6$  and a gain of energy  $E_3 = -9J$  which overcomes the loss of one singlet energy  $15/2 J$ , so that case B is favored. Furthermore, since the spin of any of the border spins is  $\mathbf{S}_b/2$  their correlation with the central one is  $-3$  in perfect agreement with Fig. 5, middle panel. Full diagonalization of the Hamiltonian for three isolated sites shows that the ground state indeed belongs to the irreducible representation with  $S_t = 3/2$  and that the local expectation values  $\langle S_i^z \rangle$  and  $\langle (S_i^z)^2 \rangle$  are very close to those shown in Fig. 5, bottom panels; this also explains that the domain wall structure first shows up in the  $S_{\text{total}}^z = 3$  sector. An analogous calculation for the spin-1/2 chain leads to  $E_3 = -3/2 J$  which is smaller than the energy loss of one singlet ( $3J$ ), and therefore case A (the well known  $S^z = 1/2$  spinons) is favored.

Increasing further the magnetic field, the magnetization curve in Fig. 6 shows another interesting feature. One finds a wide zero magnetization plateau that is stable until a metamagnetic transition takes place. This means that, upon increasing the external magnetic field  $h^z$ , at some point the Zeeman energy makes favorable some high magnetization state (with not too high energy) before selecting either the  $S_{\text{total}}^z = 1$  or the  $S_{\text{total}}^z = 3$  state described above. We have found that the magnetization jumps directly to a finite magnetization fraction  $M = 1/3$  (where  $M = 1$  means saturation). In this state

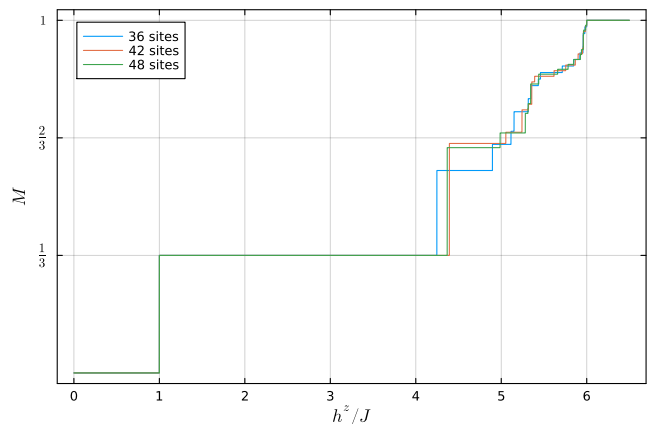


Figure 6: Magnetization curves of the magneto-elastic model, for  $\lambda = 0.18 > \lambda_c$  and three different chain lengths. Saturation magnetization is normalized to one.

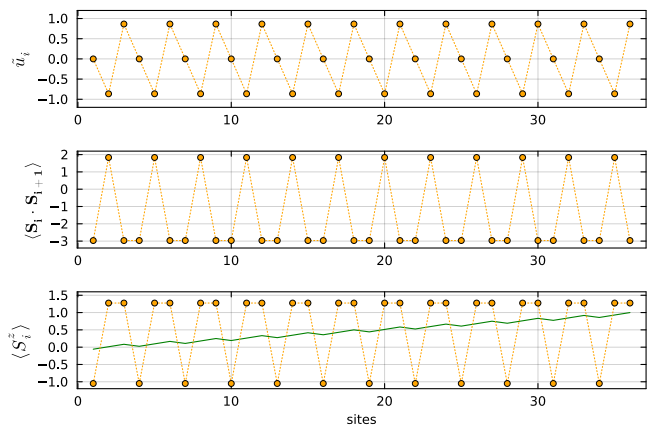


Figure 7: Local ion displacements, spin-spin correlations and local magnetization for the  $M = 1/3$  state, for  $\lambda = 0.18 > \lambda_c$ . One can see that the domain walls present in Fig. 5 now fill up the whole chain. We show in detail the  $S_{\text{total}}^z = 18$  lowest energy state in a chain of 36 sites.

the discussed  $S^z = 3/2$  spinons condensate every three sites occupying the length of the whole chain. The corresponding observable profiles are shown in Fig. 7.

The presence of a plateau and a metamagnetic jump is similar to the one found in the  $S = 1/2$  magneto-elastic chain [9,26], where bosonization arguments do explain the behavior. In contrast to that case, now the spin gap and the metamagnetic jump are seen only when  $\lambda > \lambda_c$  which is far from the perturbative region where bosonization could be applied.

The  $M = 1/3$  ordered structure is robust against the magnetic field and gives rise to a second, wider,  $M = 1/3$  plateau. For larger fields, it is not clear to us whether the magnetization curve develops smoothly or shows a third  $M = 2/3$  plateau (further investigation to be published elsewhere [29]).

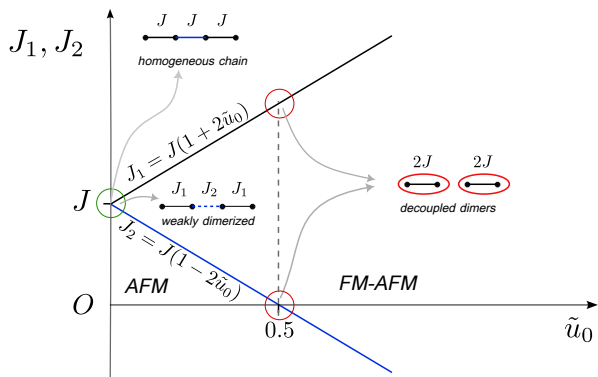


Figure 8: Dimerized exchange couplings  $J_1, J_2$  in terms of the displacement amplitude  $\tilde{u}_0$ . The null/tiny distortions found for  $\lambda < \lambda_c$  (see Fig. 3) lead to a homogeneous/weakly-dimerized antiferromagnetic spin chain (green circle region), while  $\tilde{u}_0 > 0.5$  found for  $\lambda > \lambda_c$  (red circles region) leads to an alternating (strong) antiferro- (weak) ferromagnetic spin Hamiltonian. In this phase, close to the transition,  $|J_2|/J_1 \ll 1$  allows for perturbative analysis around the decoupled dimers product state (dashed line region).

### III. ANALYTICAL INSIGHT FROM PERTURBATION THEORY

#### A. Perturbation theory in the exchange at the weak links

Motivated by the almost decoupled dimer structure found and described in the previous Section, we consider a periodic Heisenberg chain for spin  $S = 3/2$  with alternating exchange interactions.

$$\begin{aligned}
 H &= H_1 + H_2, \\
 H_1 &= J_1 \sum_{j=0}^{N/2-1} \mathbf{S}_{2j+1} \cdot \mathbf{S}_{2j+2}, \\
 H_2 &= J_2 \sum_{j=0}^{N/2-1} \mathbf{S}_{2j+2} \cdot \mathbf{S}_{2j+3}.
 \end{aligned} \quad (6)$$

For the alternating ion displacement found numerically, the exchanges are  $J_1 = J(1 + 2\tilde{u}_0)$ ,  $J_2 = J(1 - 2\tilde{u}_0)$ . Then the values  $\tilde{u}_0$  close to 0.5 found in the strongly dimerized phase correspond to the perturbative regime  $|J_2| \ll J_1$ .

The ground state to be perturbed, for  $J_2 = 0$  ( $\tilde{u}_0 \equiv 0.5$ ), consists of a direct product of singlets located on short bonds 1-2, 3-4, 5-6 ... To be precise, it is useful to use the index  $j$  in Eq. (6) to label the  $J_1$  bonds, denoting by  $|D_j : S, m\rangle$ , the eigenstates of  $J_1 \mathbf{S}_{2j+1} \cdot \mathbf{S}_{2j+2}$  with total spin  $S$  and spin projection  $m$ . The dimer singlet on bond  $j$ ,  $|D_j : 0, 0\rangle$ , can be straightforwardly constructed using the Clebsch-Gordan coefficients that combine two spins  $3/2$  to build a total spin  $S = 0$ . Similarly, excited states with total spin  $S = 1, 2, 3$  can be constructed for each bond  $j$ . The energy of these states is given by

$E_S = J_1[S(S+1)/2 - 15/4]$ . Finally the ground state of the whole chain, for  $J_2 = 0$ , reads

$$|g\rangle = \bigotimes_{j=0}^{N/2-1} |D_j : 0, 0\rangle. \quad (7)$$

One can easily see that the only non-vanishing terms to be evaluated in a perturbative computation of the ground-state energy are those involving matrix elements of the individual terms in  $H_2$ , proportional to  $J_2$ . Let us discuss the action of one of them, for example  $H_{23} = J_2 \mathbf{S}_2 \cdot \mathbf{S}_3$  on the ground state, which only acts on the neighboring dimers  $|D_0 : 0, 0\rangle$  and  $|D_1 : 0, 0\rangle$ . After a lengthy but straightforward algebra we obtain the simple result

$$\begin{aligned}
 H_{23}|D_0 : 0, 0\rangle|D_1 : 0, 0\rangle &= \frac{5\sqrt{3}J_2}{4}|e_{0,1}\rangle, \\
 |e_{0,1}\rangle &= \frac{1}{\sqrt{3}}(|D_0 : 1, 1\rangle|D_1 : 1, -1\rangle - |D_0 : 1, 0\rangle|D_1 : 1, 0\rangle \\
 &\quad + |D_0 : 1, -1\rangle|D_1 : 1, 1\rangle).
 \end{aligned} \quad (8)$$

The form of the result is expected. The state  $|e_{0,1}\rangle$ , that is the excitation between dimers 0 and 1, is a total singlet in sites 1, 2, 3, 4 obtained combining two triplets  $S = 1$  in sites 1, 2 and sites 3, 4. The vector operator  $\mathbf{S}_j$  has matrix elements only between states that differ in  $S$  by at most 1 (exactly 1 when applied to the singlet). On the other hand, since  $H_{23}$  is invariant under rotations, the singlet character of the ground state is conserved after its application to the ground state.

Using the standard equation for the energy in second order perturbation theory

$$E = E_g - \sum_e \frac{|\langle e|H_2|g\rangle|^2}{E_e - E_g}, \quad (9)$$

where  $|g\rangle$  is the ground state in Eq. (7) and  $E_g$  its energy, and similarly  $|e\rangle$ ,  $E_e$  for the excited states, the energy per site becomes

$$E_{\text{spin}} = -\frac{15}{8} \left( J_1 + \frac{5J_2^2}{J_1} \right). \quad (10)$$

While this result is quantitatively valid only for  $|J_2| \ll J_1$ , it remains qualitatively valid over a wider range, as illustrated in Fig. 9.

Returning to the dimerized magneto elastic chain, adding the elastic energy  $\tilde{u}_0^2/(2\lambda)$ , the total energy has the form

$$E_{\text{total}}/J = -A \left[ 1 + 2\tilde{u}_0 + B \frac{(1 - 2\tilde{u}_0)^2}{1 + 2\tilde{u}_0} \right] + \frac{\tilde{u}_0^2}{2\lambda}, \quad (11)$$

where  $A = 15/8$  and  $B = 5/8$ . Expanding in series of  $\tilde{u}_0$  one obtains that  $E_{\text{total}}$  can also be written in the form

$$\begin{aligned}
 E_{\text{total}}/J &= -A(1 + B) + 2A(3B - 1)\tilde{u}_0 \\
 &\quad + 8\left(\frac{1}{\lambda} - 2AB\right)\tilde{u}_0^2 + 32AB\frac{\tilde{u}_0^3}{1 + 2\tilde{u}_0}.
 \end{aligned} \quad (12)$$



This expression has a positive linear term, indicating that a small dimerization is not expected in this chain. But for large enough  $\lambda$ , the quadratic term gets negative and a first-order transition is expected, in agreement with the numerical results. The last positive term of Eq. (9) ensures the stability of the system for large  $\tilde{u}_0$ .

We have also performed the perturbative calculations for the chain with spin 1/2. The algebra is much simpler and the results are similar. In this case,  $A = 3/8$  and  $B = 1/4$ . As a consequence of the smaller value of  $B$ , the term linear in  $\tilde{u}_0$  becomes negative. This results in a finite dimerization for any  $\lambda$ , hence no first-order transition takes place, as it is well known [15].

### B. Correlation functions

The spin-spin correlation function for the chain with spin 3/2, computed as first order, provide just linear corrections. However, the matrix elements of Eq. (8) for the interactions in the weak links with exchange  $J_2$  are very large, then quadratic terms are important. To consider them in a simple analytical way, we have performed variational calculations in small clusters, which include the linear terms in  $J_2$  calculated with Eq. (8), but incorporate second-order terms, in particular taking into account the norm of the variational state.

To calculate the spin correlation in a weak link, say  $\langle \mathbf{S}_{2i+2} \cdot \mathbf{S}_{2i+3} \rangle = \langle \mathbf{S}_2 \cdot \mathbf{S}_3 \rangle$ , we consider a system of four sites 1 to 4, in which the spins 1-2 and 3-4 interact via a  $J_1 \mathbf{S}_1 \cdot \mathbf{S}_2$  and  $J_1 \mathbf{S}_3 \cdot \mathbf{S}_4$ , while 2-3 have an interaction  $J_2 \mathbf{S}_3 \cdot \mathbf{S}_4$ . We restrict to the Hilbert space of two states: the first one, which we shortly denote as  $|1\rangle = |S_{12}\rangle|S_{34}\rangle \equiv |D_0 : 0, 0\rangle|D_1 : 0, 0\rangle$ , is the product of the singlets 1-2 and 3-4 described above Eq. (8). The second one denoted by  $|2\rangle = |S_{1-4}\rangle = |e\rangle$  is the singlet obtained combining triplets 1-2 and 3-4 written in Eq. (8). Using Eq. (8), and

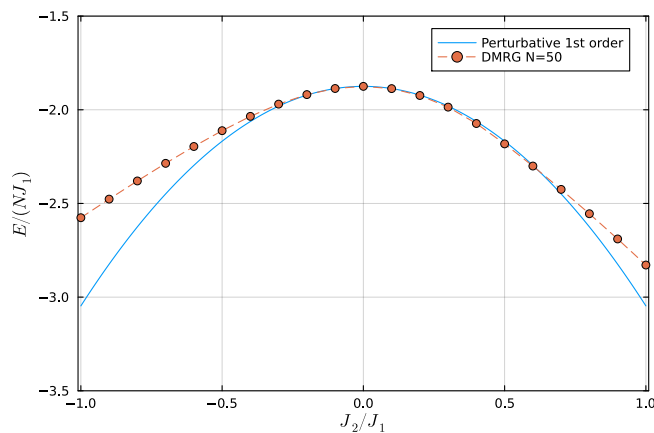


Figure 9: Comparison of DMRG results for the ground-state energy per site in a ring of 50 sites and the corresponding perturbative ones.

$$\alpha = \langle 2|\mathbf{S}_2 \cdot \mathbf{S}_3|2\rangle = -2(2 - \sqrt{3})/5, \quad (13)$$

obtained after some algebra, the Hamiltonian restricted to this subspace takes the form of the following matrix

$$\begin{pmatrix} -\frac{15}{2}J_1 & \frac{5\sqrt{3}}{4}J_2 \\ \frac{5\sqrt{3}}{4}J_2 & -\frac{11}{2}J_1 + \alpha J_2 \end{pmatrix}. \quad (14)$$

The ground state is  $|g\rangle = u|1\rangle - v|2\rangle$ , with  $u, v > 0$ ,  $u^2 + v^2 = 1$  and

$$v^2 = \frac{1}{2} - \frac{J_1 + \alpha J_2/2}{2\sqrt{(J_1 + \alpha J_2/2)^2 + 75J_2^2/16}}. \quad (15)$$

Using again Eqs. (8) and (13), the correlation in the weak links becomes

$$\langle \mathbf{S}_2 \cdot \mathbf{S}_3 \rangle = -\frac{5\sqrt{3}}{2}uv + \alpha v^2. \quad (16)$$

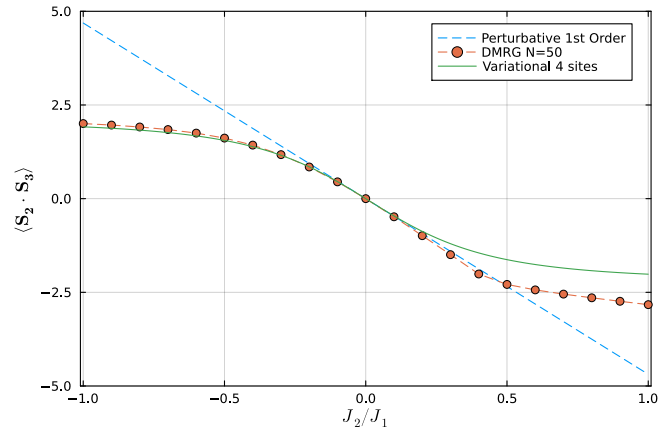


Figure 10: Spin-spin correlation function in the weak links as a function of  $J_2/J_1$ .

The result given in Eq. (16) is represented in Fig. 10 and compared with the first-order perturbative result  $-75J_2/(16J_1)$  and DMRG data. The improvement with respect to first-order perturbation is noticeable. In particular, the agreement for negative  $J_2$  with the DMRG result is remarkable.

To obtain an approximation for the correlation of the strong links one needs to follow a similar procedure as above, but for a chain of 6 sites to calculate  $\langle \mathbf{S}_3 \cdot \mathbf{S}_4 \rangle$ . Now the two relevant states have the form

$$\begin{aligned} |1\rangle &= |S_{12}\rangle|S_{34}\rangle|S_{56}\rangle, \\ |2\rangle &= \frac{1}{\sqrt{2}}(|S_{1-4}\rangle|S_{56}\rangle + |S_{12}\rangle|S_{3-6}\rangle), \end{aligned} \quad (17)$$

leading to the matrix

$$\begin{pmatrix} -\frac{45}{4}J_1 & \frac{5\sqrt{6}}{4}J_2 \\ \frac{5\sqrt{6}}{4}J_2 & -\frac{37}{2}J_1 + \alpha J_2 \end{pmatrix}. \quad (18)$$

Now the coefficient of the ground state is modified to

$$v^2 = \frac{1}{2} - \frac{J_1 + \alpha J_2/2}{2\sqrt{(J_1 + \alpha J_2/2)^2 + 150J_2^2/16}}, \quad (19)$$

and

$$\langle \mathbf{S}_3 \cdot \mathbf{S}_4 \rangle = -\frac{15}{4}u^2 - \frac{11}{4}v^2. \quad (20)$$

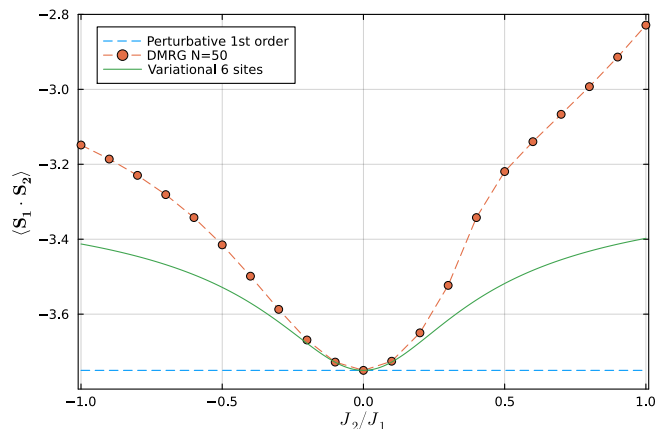


Figure 11: Spin-spin correlation function in the strong links as a function of  $J_2/J_1$ .

The result of Eq. (20) is represented in Fig. 11 and compared with DMRG calculations. To linear order in perturbation theory, there is no change in the correlation function with respect to the case  $J_2 = 0$ . The improvement introduced by the variational calculation is only qualitative in this case, indicating that it would be necessary to incorporate other second-order corrections to improve the approximation.

### C. Spin gap

To compute the energy gap, we calculate the effect of  $J_2$  up to second order in the energy of the triplet state in which all of the  $J_1$  bonds are in the singlet ground state, except one (denoted as  $B$ ), which is in the triplet state  $|B : 1, 1\rangle$ . Due to the  $SU(2)$  symmetry of the model, the energy is the same for the states with other spin projections  $|B : 1, m\rangle$ . After another lengthy calculation, a similar procedure that led to equation (8) gives

$$\begin{aligned} (H_{23}/J_2)|A : 0, 0\rangle|B : 1, 1\rangle &= -\frac{5}{4}|\alpha 11\rangle - \frac{\sqrt{10}}{4}|\beta 11\rangle \\ &+ \frac{\sqrt{10}}{2}|\gamma 11\rangle, \end{aligned} \quad (21)$$

where the second member contains the following triplet states combining a triplet state in bond  $A$  with either a singlet, triplet or quadruplet in bond  $B$

$$\begin{aligned} |\alpha 11\rangle &= |A : 1, 1\rangle|B : 0, 0\rangle, \\ |\beta 11\rangle &= \frac{1}{\sqrt{2}}(|A : 1, 0\rangle|B : 1, 1\rangle - |A : 1, 1\rangle|B : 1, 0\rangle), \\ |\gamma 11\rangle &= \sqrt{\frac{3}{5}}|A : 1, -1\rangle|B : 2, 2\rangle - \sqrt{\frac{3}{10}}|A : 1, 0\rangle|B : 2, 1\rangle \\ &- \sqrt{\frac{1}{10}}|A : 1, 1\rangle|B : 2, 0\rangle. \end{aligned} \quad (22)$$

The gap to order 0 in  $J_2$  is  $\Delta_0 = J_1$ . The first term of Eq. (21) is a hopping of the triplet to a nearest-neighbor bond. There is a second-order contribution to this hopping coming from the process  $|A : 0, 0\rangle|B : 1, 1\rangle \rightarrow |\beta 11\rangle \rightarrow |A : 1, 1\rangle|B : 0, 0\rangle$  of magnitude  $-5J_2^2/(16J_1)$  (smaller than the first one). The energy of this state is minimized creating an excitation of wave vector 0 or  $\pi$  depending on the sign of  $J_2$ , and the gain of energy is twice the effective hopping, leading to a contribution

$$\Delta_1 = -\frac{5}{4}|J_2|(2 + J_2/J_1). \quad (23)$$

The second-order processes that return to the initial state with either  $|\beta 11\rangle$  or  $|\gamma 11\rangle$  as the intermediate state, and including a factor 2 for contributions from the singlet bonds  $A$  at the left and the right of the triplet bond, contribute to the energy as

$$\Delta_\beta = \frac{-5J_2^2}{4J_1}, \quad \Delta_\gamma = \frac{-5J_2^2}{3J_1}. \quad (24)$$

Finally to obtain the gap we have to add the difference with respect to the singlet ground-state. Two contributions given by Eq. (8) are lost:

$$\Delta_s = \frac{75J_2^2}{16J_1} \quad (25)$$

Adding all contributions we obtain for the gap

$$\Delta = J_1 - \frac{5}{4}|J_2|(2 + J_2/J_1) + \frac{85J_2^2}{48J_1}. \quad (26)$$

Comparison between perturbative and DMRG results is shown in Fig. 12. The agreement is good for small  $J_2/J_1$ , particularly for positive  $J_2$ .

The very existence of the strongly dimerized FM-AFM phase, uncovered by the DMRG exploration, makes the perturbative results in the present Section a valuable tool to describe its features. Indeed the data in Fig. 3 indicate that, close to the transition,  $|J_2|/J_1$  is of the order of  $10^{-2}$  with  $J_2 < 0$ .



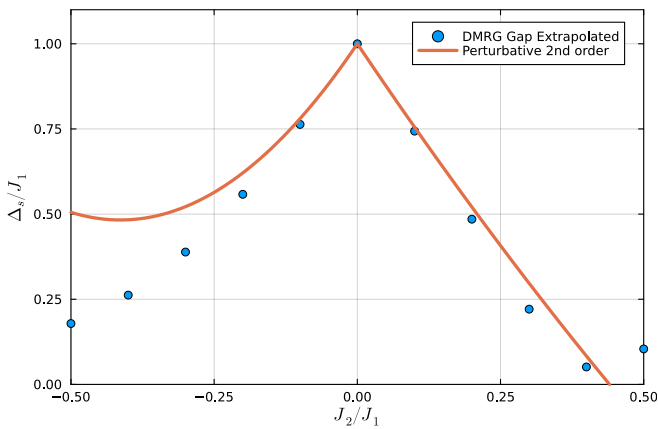


Figure 12: Comparison of extrapolated DMRG results for the spin gap and the corresponding perturbative ones.

#### IV. ABOUT THE PRESENCE OF A SPIN PEIERLS EFFECT FOR LOW SPIN-PHONON COUPLING

For low spin-phonon coupling one can use perturbative bosonization to construct a low-energy effective theory [13]. It was found [14–16] that for all half-odd integer spin there is a dimerization instability opening a spin gap  $\Delta$  which should scale as  $\Delta \propto (\tilde{u}_0)^\nu$  with  $\nu = 2/3$ . However, using perturbative bosonization [13] the exponents have been shown to increase when  $S > 1/2$ . This may explain the smallness of the spin gap and the numerical difficulties to assess its existence. In this context, numerical evidence for  $S = 1/2$ , after hard efforts, was undoubtedly settled (see for instance [30]). The spin  $3/2$  case is far more challenging and, to our knowledge, there is neither a definitive confirmation yet nor recent efforts to elucidate the question.

Soon after the bosonization prediction, this case was analyzed in Ref. [10] using exact diagonalization for systems up to 12 sites; the finite size scaling behavior of the magnetic energy gain under dimerization (for a given amplitude) suggests that it overpasses the elastic energy cost for any spring constant  $K$ , leading to an unconditional (that is, for any  $\lambda$ ) finite SP distortion in the thermodynamic limit. Recall that the similar convexity of the plots in Fig. 1 of that reference for spin  $S = 1/2$  and spin  $S = 3/2$  is the key point in arguing the existence of the spin gap. In the same spirit we have extended the analysis for larger chains up to 70 sites, now available by DMRG. The results shown in Fig. 13 confirm the current validity of their rationale.

This means that our curves in Fig. 1 should exhibit the first minimum close to, but not at  $\tilde{u}_0 = 0$ . However, due to the apparent smallness of the presumed distortion, a confident direct extrapolation to the thermodynamic limit is still unreachable within the available numerical precision.

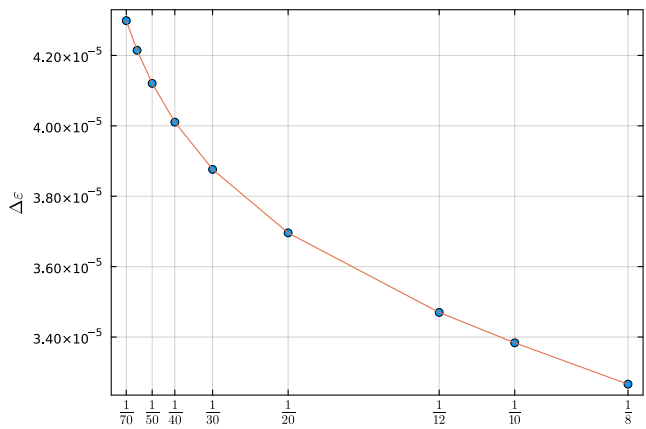


Figure 13: Size scaling of the gain in magnetic energy per site from alternating distortions with amplitude  $\tilde{\delta}_0 = 0.005$ , (update of the data in Fig. 1(c) in reference [10]). The added data points with  $12 < N \leq 70$  confirm the convexity of the plot, supporting the existence of the spin gap.

#### V. SUMMARY AND DISCUSSION

We have studied a magnetic chain coupled to the lattice for the case in which the spin at each site is  $S = 3/2$ . This value is expected in transition-metal compounds due to the effect of the Hund rules. The model, described in Section II A, contains a linear dependence of the exchange between nearest-neighbor ions with their distance, and an elastic energy loss when each ion is displaced from the equilibrium position.

In contrast to the  $S = 1/2$  case, we find a first-order transition as a function of the dimensionless spin-phonon coupling  $\lambda$  at a critical value  $\lambda_c$ . Our numerical results are consistent with a vanishing or very small dimerization for  $\lambda < \lambda_c$ , although from complementary studies we expect a small dimerization.

Instead, for  $\lambda > \lambda_c$  there is a strong dimerization, with large and small alternating exchange interactions  $J_1$  and  $J_2$ . The latter can even be negative within our model in this dimerized phase. While this is not expected for example in the superexchange for spins  $1/2$  in the cuprates as the distance increases, a change in the sign of the superexchange with structural parameters has been found by theory and experiment in doped spin-1  $1T\text{-CrSe}_2$  [31]. The strongly dimerized phase is characterized by correlation functions  $\langle \mathbf{S}_i \cdot \mathbf{S}_{i+1} \rangle$  near the ideal ones  $-15/4$  for singlet dimers for the strong bonds, and small, in general negative values for the weak bonds. In particular,  $J_2$  vanishes at the transition, rendering a system of perfectly decoupled singlet dimers.

When a magnetic field is included in the strongly dimerized phase, solitons separating the two possible dimerized phases (odd or even strong bonds) are formed.

In the strongly dimerized phase, the large spin gap means the system does not gain as much energy from the applied magnetic field  $h^z$  compared to the non-dimerized

or weakly dimerized phase. This renders it possible to induce the transition with an external  $h^z$ , which could be relevant for applications. In many cases, distortions are associated with ferroelectricity and in this case, they could be significantly reduced by an external magnetic field. Conversely, an applied electric field could induce ferroelectricity and destroy the magnetic phase. Another possibility is to tune  $\lambda$  by striction or alloying.

### Acknowledgements

CJG is partially supported by CONICET (PIP 3220), Argentina. AAA acknowledges financial support pro-

vided by PICT 2020A 03661 and PICT 2018-01546 of the Agencia I+D+i, Argentina. AOD is partially supported by UNR (80020190300213UR), Argentina. GLR and DCC are partially supported by CONICET (PIP 1146), Argentina.

- 
- <sup>1</sup> M.C. Cross and D.S. Fisher, *A new theory of the spin-Peierls transition with special relevance to the experiments on TTFCuBDT*, Phys. Rev. B **19**, 402 (1979).
- <sup>2</sup> A. E. Feiguin, J. A. Riera, A. Dobry, and H. A. Ceccatto, *Numerical study of the incommensurate phase in spin-Peierls systems*, Phys. Rev. B **56**, 14607 (1997).
- <sup>3</sup> J. Riera and A. Dobry, *Magnetic susceptibility in the spin-Peierl system CuGeO<sub>3</sub>*, Phys. Rev. B **51**, 16098 (1995).
- <sup>4</sup> K. Penc, N. Shannon, and H. Shiba, *Half-Magnetization Plateau Stabilized by Structural Distortion in the Antiferromagnetic Heisenberg Model on a Pyrochlore Lattice* Phys. Rev. Lett. **93**, 197203 (2004).
- <sup>5</sup> D.L. Bergman, R. Shindou, G.A. Fiete, and L. Balents, *Models of degeneracy breaking in pyrochlore antiferromagnets* Phys. Rev. B **74**, 134409 (2006).
- <sup>6</sup> J.-P. Pouget, *Spin-Peierls, Spin-Ladder and Kondo Coupling in Weakly Localized Quasi-1D Molecular Systems: An Overview*. Magnetochemistry **9**, 57 (2023).
- <sup>7</sup> M. Hase, I. Terasaki, and K. Uchinokura, *Observation of the spin-Peierls transition in linear Cu<sup>2+</sup> (spin-1/2) chains in an inorganic compound CuGeO<sub>3</sub>* Phys. Rev. Lett. **70**, 3651 (1993).
- <sup>8</sup> V. Kiryukhin, B. Keimer, J. P. Hill, S. M. Coad, and D. M. Paul *Synchrotron x-ray-scattering study of magnetic-field-induced transitions in Cu<sub>1-x</sub>(Zn, Ni)<sub>x</sub>GeO<sub>3</sub>* Phys. Rev. B, **54**, 7269 (1996)
- <sup>9</sup> C.J. Gazza, A.O. Dobry, D.C. Cabra, and T. Vekua, *Excitations with fractional spin less than 1/2 in frustrated magnetoelastic chains*, Phys. Rev. B **75**, 165104 (2007).
- <sup>10</sup> D. Guo, T. Kennedy, and S. Mazumdar, *Spin-Peierls transitions in S>1/2 Heisenberg chains*, Phys. Rev. B **41**, 9592 (1990).
- <sup>11</sup> C.H. Aits, U. Löw, A. Klümper, and W. Weber *Structural and magnetic instabilities of two-dimensional quantum spin systems* Phys. Rev. B **74**, 014425 (2006); Chenglong Jia, Jung Hoon Han *Spin-lattice interaction effect in frustrated antiferromagnets* Physica B **378–380**, 884 (2006).
- <sup>12</sup> F.D.M. Haldane, *Nonlinear Field Theory of Large-Spin Heisenberg Antiferromagnets: Semiclassically Quantized Solitons of the One-Dimensional Easy-Axis Néel State*, Phys. Rev. Lett. **50** 1153 (1983).
- <sup>13</sup> H. J. Schulz, *Phase diagrams and correlation exponents for quantum spin chains of arbitrary spin quantum number*, Phys. Rev. B **34**, 6372 (1986).
- <sup>14</sup> I. Affleck and F.D.M. Haldane, *Critical theory of quantum spin chains*, Phys. Rev. B **36**, 5291 (1987).
- <sup>15</sup> I. Affleck, D. Gepner, H. J. Schulz and T. Ziman, *Critical behaviour of spin-s Heisenberg antiferromagnetic chains: analytic and numerical results*, Journal of Physics A: Mathematical and General, **22**(5), 511 (1989).
- <sup>16</sup> D. C. Cabra, P. Pujol, and C. von Reichenbach, *Non-Abelian bosonization and Haldane’s conjecture*, Phys. Rev. B **58**, 65 (1998).
- <sup>17</sup> *Magnetic order and magnetoelectric properties of R<sub>2</sub>CoMnO<sub>6</sub> (double) perovskites*, J. Blasco, J.L. García-Muñoz, J. García, G. Subías, J. Stankiewicz, J.A. Rodríguez-Velamazán, and C. Ritter, Phys. Rev. B **96**, 024409 (2017).
- <sup>18</sup> *Multiferroic behavior in the double-perovskite Lu<sub>2</sub>MnCoO<sub>6</sub>*, S. Yáñez-Vilar, E.D. Mun, V.S. Zapf, B.G. Ueland, J.S. Gardner, J.D. Thompson, J. Singleton, M. Sánchez-Andújar, J. Mira, N. Biskup, M.A. Señarís-Rodríguez, and C.D. Batista, Phys. Rev. B **84**, 134427 (2011).
- <sup>19</sup> *Electric polarization observed in single crystals of multiferroic Lu<sub>2</sub>MnCoO<sub>6</sub>*, S. Chikara, J. Singleton, J. Bowlan, D.A. Yarotski, N. Lee, H.Y. Choi, Y.J. Choi, and V.S. Zapf, Phys. Rev. B **93**, 180405(R) (2016).
- <sup>20</sup> *Strong magnetoelectric coupling in mixed ferrimagnetic-multiferroic phases of a double perovskite*, M.K. Kim, J.Y. Moon, S.H. Oh, D.G. Oh, Y.J. Choi, and N. Lee, Scientific Reports **9**, 5456 (2019).
- <sup>21</sup> *Magnetic domain wall induced ferroelectricity in double perovskites*, H.Y. Zhou, H.J. Zhao, W.Q. Zhang, and X.M. Chen, Appl. Phys. Lett. **106**, 152901 (2015).
- <sup>22</sup> D.C. Cabra, A.O. Dobry, C.J. Gazza, and G. L. Rossini, *Microscopic model for magnetoelectric coupling through lattice distortions*, Phys. Rev. B **100**, 161111(R) (2019); *Topological solitons and bulk polarization switch in collinear type-II multiferroics*, Phys. Rev. B **103**, 144421 (2021); *Double frustration and magnetoelectroelastic excitations in collinear multiferroic materials*, Phys. Rev. B **105**, 115103 (2022).
- <sup>23</sup> L. Pili, R.A. Borzi, D.C. Cabra, and S.A. Grigera, *Simple microscopic model for magneto-electric coupling in type-II antiferromagnetic multiferroics*, Phys. Rev. B **105**, 094428 (2022).
- <sup>24</sup> *The ITensor Software Library for Tensor Network Cal-*

- culations, M. Fishman, S.R. White and E. Miles Stoudenmire, SciPost Phys. Codebases, 4, 2022, URL <https://scipost.org/10.21468/SciPostPhysCodeb.4>
- <sup>25</sup> D. C. Cabra, A. Honecker, and P. Pujol, *Magnetization plateaux in N-leg spin ladders*, Phys. Rev. B **58**, 6241 (1998).
- <sup>26</sup> T. Vekua, D. C. Cabra, A. Dobry, C. Gazza, and D. Poilblanc, *Magnetization Plateaus Induced by a Coupling to the Lattice*, Phys. Rev. Lett. **96**, 117205 (2006).
- <sup>27</sup> For large enough  $\lambda$  we found a portion of the chain with a pronounced length contraction, ordered as in the present model, accompanied by a disordered portion with more separated ions to satisfy the total length constraint.
- <sup>28</sup> F. Wang and A. Vishwanath, *Spin phonon induced col-*
- inear order and magnetization plateaus in triangular and kagome antiferromagnets. Applications to CuFeO<sub>2</sub>*, Phys. Rev. Lett. **100**, 077201 (2008).
- <sup>29</sup> The authors, in preparation.
- <sup>30</sup> M. Kumar, S. Ramasesha, D. Sen, and Z.G. Soos, *Scaling exponents in spin 1/2 Heisenberg chains with dimerization and frustration studied with the density-matrix renormalization group*, Phys. Rev. B **75**, 052404 (2007).
- <sup>31</sup> D. C. Freitas, M. Núñez, P. Strobel, A. Sulpice, R. Weht, A. A. Aligia, and M. Núñez-Regueiro, *Antiferromagnetism and Ferromagnetism in Layered 1T-CrSe<sub>2</sub> with V and Ti replacements*, Phys. Rev. B **87**, 014420 (2013).